Tricyclic [1,2,4]Triazine 1,4-Dioxides As Hypoxia Selective Cytotoxins

Michael P. Hay,* Kevin O. Hicks, Karin Pchalek,† Ho H. Lee, Adrian Blaser, Frederik B. Pruijn, Robert F. Anderson, Sujata S. Shinde, William R. Wilson, and William A. Denny

Auckland Cancer Society Research Centre, Faculty of Medical and Health Sciences, The University of Auckland, Auckland, New Zealand

Received July 30, 2008

A series of novel tricyclic triazine-di-*N*-oxides (TTOs) related to tirapazamine have been designed and prepared. A wide range of structural arrangements with cycloalkyl, oxygen-, and nitrogen-containing saturated rings fused to the triazine core, coupled with various side chains linked to either hemisphere, resulted in TTO analogues that displayed hypoxia-selective cytotoxicity in vitro. Optimal rates of hypoxic metabolism and tissue diffusion coefficients were achieved with fused cycloalkyl rings in combination with both the 3-aminoalkyl or 3-alkyl substituents linked to weakly basic soluble amines. The selection was further refined using pharmacokinetic/pharmacodynamic model predictions of the in vivo hypoxic potency (AUC_{req}) and selectivity (HCD) with 12 TTO analogues predicted to be active in vivo, subject to the achievement of adequate plasma pharmacokinetics.

Introduction

The increasingly well-defined role of tumor hypoxia in driving tumor metabolism, progression, invasion, and metastasis,[1−7] as well as resistance to therapy,[8−13] emphasizes the cogent need for clinical agents that selectively target hypoxia.[14,15]

One class of hypoxia-selective cytotoxins under development is the benzotriazine 1,4-dioxides (BTOs) represented by the archetype tirapazamine (**1**, TPZ).[a16,17] TPZ acts as a prodrug that undergoes selective bioreductive activation[18] under hypoxic conditions to ultimately form an oxidizing radical that may react with DNA,[19−22] leading to DNA strand breaks and poisoning of topoisomerase II.[23−27] TPZ shows selective toxicity to hypoxic cells in vitro and in experimental tumors,[17,28−31] and a range of clinical trials have produced modest therapeutic results to date.[32−34] This approach, using TPZ to selectively kill hypoxic cells in tumors, is an early example of "physiologically-targeted therapy." Recent prognostic data[35,36] from a clinical trial in head and neck cancer[37] has highlighted the importance of preselecting patients with hypoxia when using such a targeted therapy, and this may in part explain the modest results with TPZ in trials.

TPZ has limitations that blunt its efficacy in vivo and, potentially, in the clinic. It displays lower hypoxic selectivity in vivo (2- to 3-fold) compared to in vitro (hypoxic cytotoxicity ratio, HCR, ca. 50- to100-fold),[38] which has been ascribed to rapid metabolism of TPZ in hypoxic tissues, leading to limited penetration of the drug into hypoxic tissue.[39−45]

Overcoming this limited extravascular transport (EVT) requires balancing the rate of bioreductive metabolism relative to the tissue diffusion coefficient: analogues with low rates of bioreductive metabolism lack cytotoxic potency, while analogues with high rates of metabolism suffer limited EVT due to excessive consumption of the prodrug.[40,46−49] Optimisation of EVT is but one element required in maximizing activity against hypoxic cells in tumors. We have recently demonstrated a spatially resolved pharmacokinetic/pharmacodynamic (PK/PD) model that integrates hypoxic cytotoxicity and selectivity, EVT, and plasma pharmacokinetics to successfully predict in vivo activity against hypoxic cells in HT29[45] and SiHa tumors.[46] We have applied this model to guide drug synthesis and testing in two studies of BTO analogues and identified several BTOs with improved activity against hypoxic cells in vivo.[48,49]

We initially determined structure−activity relationships (SAR) between A-ring substituents and one-electron reduction potential [$E(1)$], hypoxic cytotoxicity, and hypoxic selectivity,[50] but issues of aqueous solubility and EVT were not addressed directly in this study. Another study of neutral BTOs demonstrated an increase in tissue diffusion coefficients, measured using multicellular layer (MCL) cultures of analogues with increased lipophilicity.[47] Recently, we reported[48] a systematic evaluation of 3-aminoalkylamino BTOs, seeking analogues with improved aqueous solubility and EVT. This study showed that electron-donating substituents in the 6-position could be used to counteract increased rates of metabolism caused by the 3-aminoalkylamino substituents, e.g., **2**, and demonstrated that sufficiently lipophilic analogues provide MCL penetration similar to TPZ and show activity against hypoxic cells in tumor xenografts. A subsequent study[49] demonstrated that removal of hydrogen bond donors at the 3-position could further increase tissue diffusion coefficients but that the less electron-donating 3-alkyl substituents raised reduction potentials and hypoxic metabolism, which could be counteracted by adding electron-donating substituents to the A-ring. Several BTO analogues with improved in vivo activity relative to TPZ were identified in these studies.

However, these findings and the limited SAR studies by others[51−55] have all been on analogues based on the 1,2,4-

* To whom correspondence should be addressed. Phone: 64-9-9235698, ext. 86598. Fax: 64-9-3737502. E-mail: m.hay@auckland.ac.nz. Address: Auckland Cancer Society Research Centre, Faculty of Medical and Health Sciences, The University of Auckland, Private Bag 92019, Auckland 1142, New Zealand.

† Current address: Boehringer Ingelheim Pharma GmbH & Co. KG, 55216 Ingelheim am Rhein, Germany.

[a] Abbreviations: TPZ, Tirapazamine; BTO, 1,2,4-benzotriazine 1,4-dioxide; HCR, hypoxic cytotoxicity ratio; EVT, extravascular transport; $E(1)$, one-electron reduction potential; PK/PD, pharmacokinetic/pharmacodynamic; D, tissue diffusion coefficient; MCL, multicellular layer; k_{met}, first-order rate constant for bioreductive metabolism; SAR, structure−activity relationships; 9-BBN, 9-borabicyclo[3.3.1]nonane; $P_{7.4}$, octanol/water coefficient at pH 7.4; CT_{10}, area under concentration−time curve providing 10% surviving fraction; M_{10}, amount of BTO metabolized for 10% surviving fraction; $X_{1/2}$, calculated penetration half-distance into hypoxic tissue; SF, surviving fraction; LCK, log cell kill; AUC_{req}, area under the plasma concentration−time curve required to give 1 log of cell kill of hypoxic cells in HT29 tumors; HCD, hypoxic cytotoxicity differential.

10.1021/jm800967h CCC: $40.75 © 2008 American Chemical Society
Published on Web 10/11/2008

Scheme 1[a]

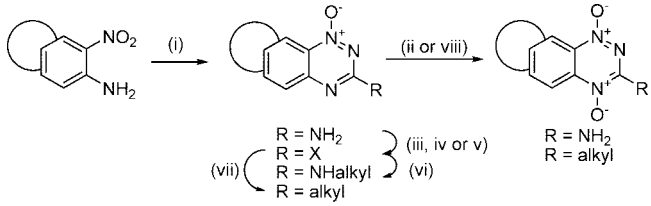

[a] Reagents: (i) NH_2CN, HCl, Δ, then 30% NaOH, Δ; (ii) CH_3CO_3H, CH_3CO_2H; (iii) $NaNO_2$, CF_3CO_2H; (iv) DMF, $POCl_3$, Δ; (v) *t*-$BuNO_2$, CH_2I_2, CuI, THF, Δ; (vi) $R_2CH_2CH_2NH_2$, DME, Δ; (vii) Stille or Heck coupling; (viii) CF_3CO_3H, CF_3CO_2H, DCM.

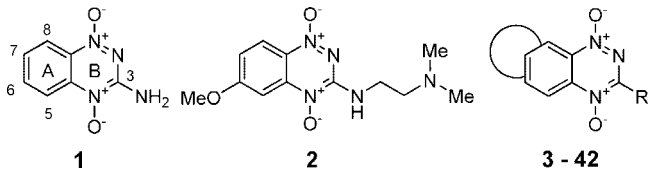

Figure 1

benzotriazine 1,4-dioxide core. With the exception of several studies on the parent 1,2,4-triazine dioxides[56,57] and isosteric cyanoquinoxaline 1,4-dioxides,[58−61] there has been little exploration of related heterocyclic dioxides as hypoxia-selective cytotoxins. In this study, we have synthesized 40 novel tricyclic triazine 1,4-dioxides (TTOs) **3**−**42** (Figure 1) and examined their in vitro activity as hypoxia-selective cytotoxins. We have focused on using lipophilic ring systems of an electron-donating nature in an effort to increase EVT by more rapid diffusion through tumor tissue and reduced rates of hypoxic metabolism. We have used in vitro PK/PD modeling to assess the effect of the structural changes on EVT, and this approach has identified 20 novel TTOs of diverse structure with promising in vitro profiles as hypoxia-selective cytotoxins.

Chemistry

Synthesis. Our synthetic strategies build on well established methodology for the formation of the 3-amino-1,2,4-benzotriazine 1-oxide core[48,50] and elaboration to 3-alkyl analogues,[62,63] and these general methods are described below. Bicyclic nitroanilines were treated with cyanamide and cHCl to generate the intermediate guanidines, which were cyclized under strongly basic conditions to give 3-aminotriazine 1-oxides (Scheme 1). Oxidation of 3-aminotriazine 1-oxides to 3-amino TTOs was achieved with peracetic acid. Conversion of 3-aminotriazine 1-oxides to 3-chlorotriazine 1-oxides was achieved by diazotization in trifluoroacetic acid, followed by chlorination of the intermediate phenol. Displacement of 3-chlorides with a variety of amines gave the 3-aminoalkyltriazine 1-oxides. 3-Aminotriazine 1-oxides were also converted to 3-iodides by diazotization with *t*$BuNO_2$ in THF and iodination with CH_2I_2. Reaction of 3-halotriazines with various stannanes using Stille conditions gave 3-alkyltriazine 1-oxides. Alternatively, reaction of 3-iodides with allyl alcohol under Heck conditions gave 3-alkyltriazine 1-oxides. Oxidation of 3-substituted triazine 1-oxides with trifluoroperactic acid, using an excess of trifluoroacetic acid to protect any aliphatic amines present, gave a variety of TTOs.

In particular, our first set of targets included cyclopentane-, cyclohexane-, and cycloheptane-fused benzotriazine dioxides with a range of 3-aminoalkyl substituents bearing solubilizing side chains. Thus, acetylation of 5-aminoindane (**43**) gave acetamide **44**, which was nitrated to give isomeric nitroacetamides **45**−**47** (Scheme 2). Deprotection of nitroacetamide **45** under acidic conditions gave nitroaniline **48**, which underwent Arndt cyclization to give 1-oxide **49**, which was oxidized to TTO **3**. The 1-oxide **49** was converted to the 3-chloride **50**, and this underwent displacement with a series of lipophilic aminoalkylamines to give 1-oxides **51**−**55**, which were oxidized to the corresponding TTOs **4**−**8**.

A similar sequence of reactions was carried out using the angular nitroacetamide isomer **46**. Deprotection gave nitroaniline **56**, which was converted to 1-oxide **57** and then to 3-chloride **58**, which was elaborated to a series of 3-aminoalkyl 1-oxides **59**−**63** and oxidized to TTOs **9**−**13**, respectively.

Access to the methylcyclopentane analogues **14** and **15** was accomplished by elaboration of 2-methylindanone **64** (Scheme 3). Nitration gave 4- and 6-nitroisomers **65** and **66**. Reduction and acetylation of **66** gave acetamide **67**, which was nitrated to give nitroacetamide **68** and deprotected to nitroaniline **69**. Cyclization of **69** gave 1-oxide **70**, which was diazotized and chlorinated to 3-chloride **71**. Displacement with amines gave **72** and **73**, which were oxidized to TTOs **14** and **15**, respectively.

Similar sequences were followed to elaborate α-tetralone (**74**) to linear tricyclic 1,4-dioxides **16** and **17** and the angular analogue **18** (Scheme 4) as well as to convert benzosuberone (**88**) to the cycloheptane TTO **19** (Scheme 5).

The use of alkoxy substituents to lower electron affinity has previously[48,49] yielded active analogues, e.g., **2**, thus a series of fused dihydrobenzofuran analogues were synthesized (Scheme 6). Friedel−Crafts acylation of dihydrobenzofuran (**96**) gave ketone **97**, which was converted to the oxime and underwent Beckmann rearrangement to acetamide **98**. Nitration gave nitroacetamide **99**, which was deprotected to give nitroaniline **100**. Conversion of **100** to the "[3,2-*g*]" 3-amino 1-oxide isomer **101** and subsequent chlorination gave 3-chloride **102**, which underwent displacement with amines to give 1-oxides **103** and **104**, which were oxidized to the TTOs **20** and **21**, respectively.

Access to the "[2,3-*g*]" isomer pattern was achieved by diazotization of nitroaniline **100** in the presence of H_3PO_2, reduction of the resulting nitrobenzofuran **105** to the intermediate aniline, and protection as the acetamide **106**, and nitration and deprotection to give nitroaniline **107**. Cyclization gave the isomeric BTO 1-oxide **108**, which was directly oxidized to the 1,4-dioxide **22** or elaborated, via the chloride **109**, to 3-aminoalkylamino 1-oxides **110**−**112** and subsequently to the corresponding TTOs **23**−**25**.

The acetamide **114** of 3,4-methylenedioxoaniline (**113**) underwent nitration to give nitroacetamide **115**, which was deprotected to give nitroaniline **116** (Scheme 6). Cyclization of **116** gave the 1-oxide **117**, which was converted to the 3-chloride **118**, displaced with amine side chain to give **119** and oxidized to TTO **26**.

Nitration of 4-chromanone (**120**) gave predominantly the 6-nitro isomer **122**, which was reduced and acetylated to give acetamide **123** in moderate (56%) yield (Scheme 7). Alternatively, zinc reduction of **120** gave chroman **124**, which underwent Friedel−Crafts acylation to give **125** with subsequent oxime formation and Beckmann rearrangement to **123**. Although lower yielding (41%), this route was more convenient on a large scale. Nitration of **123** gave a ca. 1:1 ratio of the two isomeric nitroacetamides **126** and **127**, which were deprotected to give corresponding nitroanilines **128** and **133**. Cyclization of **128** gave 1-oxide **129**, which was converted, via chloride **130**, to 1-oxides **131** and **132** and subsequently oxidized to 1,4-dioxides **27** and **28**. A similar sequence converted the isomeric nitroaniline **133** to TTO **29**.

Scheme 2[a]

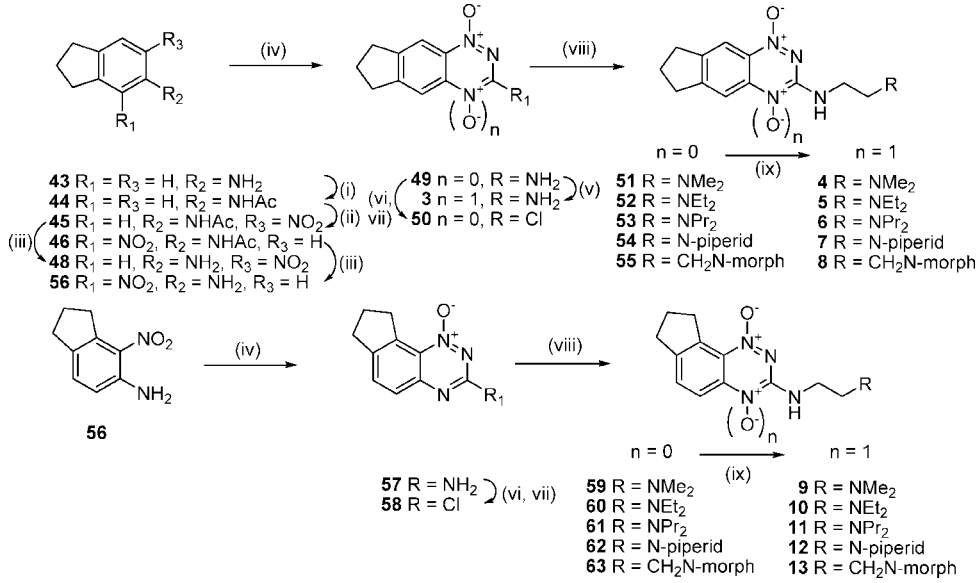

[a] Reagents: (i) Ac_2O, dioxane; (ii) KNO_3, H_2SO_4; (iii) 5 M HCl, Δ; (iv) NH_2CN, HCl, Δ, then 30% NaOH, Δ; (v) CH_3CO_3H, CH_3CO_2H; (vi) $NaNO_2$, CF_3CO_2H; (vii) DMF, $POCl_3$, Δ; (viii) $RCH_2CH_2NH_2$, DME, Δ; (ix) CF_3CO_3H, CF_3CO_2H, DCM.

Scheme 3[a]

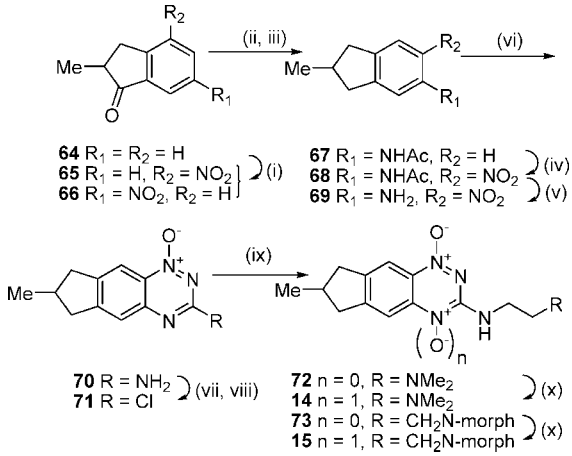

[a] Reagents: (i) $cHNO_3$; (ii) H_2, Pd/C, cHCl, EtOH; (iii) Ac_2O, dioxane; (iv) $cHNO_3$, CF_3CO_2H; (v) cHCl, EtOH, Δ; (vi) NH_2CN, HCl, Δ, then 30% NaOH, Δ; (vii) $NaNO_2$, CF_3CO_2H; (viii) DMF, $POCl_3$, Δ; (ix) $RCH_2CH_2NH_2$, DME, Δ; (x) CF_3CO_3H, CF_3CO_2H, DCM.

Scheme 4[a]

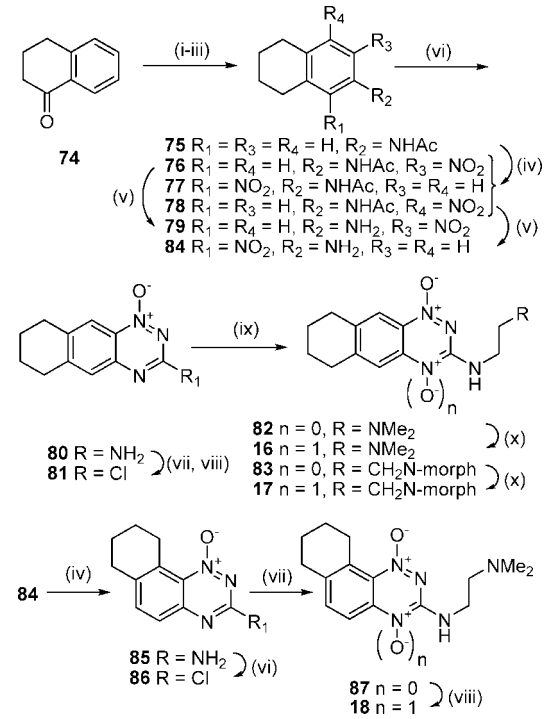

[a] Reagents: (i) $fHNO_3$, H_2SO_4; (ii) H_2, Pd/C, cHCl, EtOH; (iii) Ac_2O, dioxane; (iv) KNO_3, H_2SO_4; (v) 5 M HCl, Δ; (vi) NH_2CN, HCl, Δ, then 30% NaOH, Δ; (vii) $NaNO_2$, CF_3CO_2H; (viii) DMF, $POCl_3$, Δ; (ix) $RCH_2CH_2NH_2$, DME, Δ; (x) CF_3CO_3H, CF_3CO_2H, DCM.

Recent work[49] had shown that analogues with a soluble side chain appended to the benzo ring of BTOs displayed excellent hypoxic cytotoxicity and selectivity, so we explored analogues with solubilizing functionality linked to, or part of, the saturated ring of the TTOs. Thus mesylation of 2-indanol (**137**) and displacement with dimethylamine gave amine **138**, which was nitrated to give 5-nitroindanamine **139** (Scheme 8). Reduction and acetylation gave **140**, nitration of which gave an inseparable mixture of nitroacetamide isomers. Deprotection and fractional crystallization gave the single nitroaniline isomer **141** in 50% yield for the two steps. Cyclization of **141** gave 1-oxide **142**, which was converted to 3-chloride **143**, displaced with ethylamine to give 3-amine **144**, and selectively oxidized to TTO **30**.

Nitration of bis(bromomethyl)benzene (**145**) gave 4-nitrobenzene **146**, which was cyclized to 2-ethylisoindole **147**. Reduction of **147** and acetylation gave acetamide **148**, which was nitrated and deprotected to give nitroaniline **150**. Cyclization of **150** gave 1-oxide **151**, which was oxidized to TTO **31**. Reductive amination of 7-nitro-tetrahydroisoquinoline **152** with acetic formic anhydride gave **153**. Reduction of the nitro group and protection gave acetamide **154**, nitration of which gave an inseparable mixture of nitroacetamides. Deprotection allowed purification of the isomeric nitroanilines **155** and **156**. Cyclization of nitroaniline **156** gave 1-oxide **157**, which was converted to TTO **32** in a similar manner to **142**.

3-Alkyl BTOs displayed increased hypoxic potency compared to the analogous 3-aminoalkyl BTOs but often had reduced aqueous solubility.[49] To avoid this limitation with analogous

Scheme 5[a]

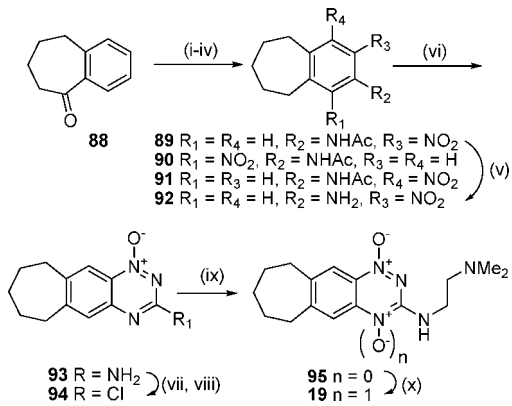

[a] Reagents: (i) $fHNO_3$, cH_2SO_4; (ii) H_2, Pd/C, cHCl, EtOH; (iii) Ac_2O, dioxane; (iv) KNO_3, H_2SO_4; (v) 5 M HCl, Δ; (vi) NH_2CN, HCl, Δ, then 30% NaOH, Δ; (vii) $NaNO_2$, CF_3CO_2H; (viii) DMF, $POCl_3$, Δ; (ix) $Me_2NCH_2CH_2NH_2$, DME, Δ; (x) CF_3CO_3H, CF_3CO_2H, DCM.

TTOs, we sought to maintain aqueous solubility by attaching a solubilizing moiety via the 3-position or attached to the third (saturated) ring of the TTO. Diazotization of the 3-amino 1-oxide **70** and reaction with CH_2I_2 gave the iodide **160**, which underwent a Heck reaction with allyl alcohol using $Pd(OAc)_2$ as the catalyst to give aldehyde **161** (Scheme 9). Reductive amination with morpholine gave both the terminal alcohol **162** as well as the tertiary morpholide **163**. Oxidation of alcohol **162** and amine **163** gave TTOs **33** and **34**, respectively.

Two routes were explored to synthesize nitroaniline **168** (Scheme 10). Reaction of 1,2-bis(bromomethyl)-4-nitrobenzene (**146**) with diethyl malonate, with subsequent hydrolysis and decarboxylation giving indane-2-carboxylic acid **164**, which was reduced to the corresponding alcohol **165**, protected as the *N*,*O*-diacetyl compound **166** and nitrated to give nitroacetamide **167**. Low yields in the first steps of this sequence prompted us to explore an alternative. Thus, hydrolysis of nitrile **174** gave the carboxylic acid **175**, nitration of which gave an inseparable mixture of isomeric nitroindane 2-carboxylic acids **164** and **176**. Reduction of this mixture gave a mixture of alcohols **165** and **177**, which underwent further reduction, protection as the *N*,*O*-diacetyl compounds, and subsequent nitration to give nitroacetamide **167** in 37% overall yield for the six steps. Deprotection of **167** gave nitroaniline **168**, which was cyclized to 3-amino 1-oxide **169**. Protection of 1-oxide **169** as the TBDMS ether **170** and iodination gave 3-iodide **171**, which underwent Stille coupling with $SnEt_4$ and $Pd(PPh_3)_4$ to give the 3-ethyl derivative **173**. Oxidation and simultaneous deprotection of **173** gave TTO **35**. The 3-ethyl silyl ether **173** was also deprotected to alcohol **178**, and reaction with mesyl chloride and morpholine gave the tertiary amine **179**. Selective aromatic *N*-oxidation of **179** gave TTO **36**.

Similarly, Stille reaction of **171** with allyltributyltin gave alkene **180**, which underwent hydroboration with 9-borabicyclo[3.3.1]nonane (9-BBN) to give the primary alcohol **181** (Scheme 11). Mesylation of **181** and displacement by morpholine gave amine **182**, which was deprotected to alcohol **183** and oxidized to TTO **37**.

Condensation of indanone **184** with glyoxylic acid gave the enone acid **185**, which was reduced to acid **186** (Scheme 12). Esterification of **186**, reduction to the alcohol **188** with $LiAlH_4$, and acetylation gave **189**. Nitration of **189** gave a mixture of nitro isomers **190** and **191**, which were reduced to the corresponding acetamides **192** and **193**. Further nitration of the mixture gave the single isomer **194**, which was deprotected to give nitroaniline **195**. Cyclization of **195** gave 1-oxide **196**, which was diazotized and converted to the 3-iodide **197**. Protection of the side chain as the THP ether **198** allowed Stille coupling to form 3-ethyl 1-oxide **199**. Deprotection of the THP ether gave alcohol **200**, which was oxidized to TTO **38**. Alcohol **200** was further functionalized by reaction with mesyl chloride and morpholine to give morpholide **201**, which was selectively oxidized to TTO **39**.

A series of 3-alkyl TTOs were also explored bearing heterocyclic saturated rings to potentially balance the effect of the 3-alkyl group on reduction potential and consequently rates of hypoxic metabolism. Conversion of dihydrofuran 1-oxide **108** to the iodide **109** followed by Heck coupling with allyl alcohol gave aldehyde **203** (Scheme 13). This aldehyde underwent reductive amination to give amine **204**, which was oxidized to TTO **40**. Stille reaction of the tetrahydroisoquinoline 3-chloride **158** gave the 3-ethyl 1-oxide **205**, which was oxidized to TTO **41**. Cyclization of the nitroaniline **155** gave the 1-oxide **206**, which was converted to the chloride **207**. Stille coupling to gave 3-ethyl 1-oxide **208**, which was oxidized to TTO **42**.

One Electron Reduction Potential Measurements, *E*(1). Pulse radiolysis experiments were performed on the University of Auckland Dynaray 4 (4 MeV) linear accelerator (200 ns pulse length with a custom-built optical radical detection system).[64] *E*(1) values for the TTOs were determined in anaerobic aqueous solutions containing 2-propanol (0.1 M) buffered at pH 7.0 (10 mM phosphate) by measuring the equilibrium constant for the electron transfer between the radical anions of the compounds and the appropriate viologen or quinone reference standard.[65] Data were obtained at three concentration ratios at room temperature (22 ± 2 °C) and used to calculate the Δ*E* between the compounds and references, allowing for ionic strength effects on the equilibria.

Physicochemical Measurements. Solubilities of the TTOs **3**−**42** were determined in culture medium containing 5% fetal calf serum at 22 °C. Octanol/water partition coefficients were measured at pH 7.4 ($P_{7.4}$) for TPZ, **2**, and a subset of four TTOs by a low volume shake flask method, with TTO concentrations in both the octanol and buffer phases analyzed by HPLC as previously described.[48,66] These values, in conjunction with previously determined values for related BTOs,[47−50] were used to "train" ACD LogP/LogD prediction software (v. 8.0, Advanced Chemistry Development Inc., Toronto, Canada) using a combination of ACD/LogP System Training and Accuracy Extender. Apparent (macroscopic) pK_a values for the side chain were calculated using ACD pK_a prediction software (v. 8.0, Advanced Chemistry Development Inc., Toronto, Canada).

Biological Assays. Cytotoxic potency was determined by IC_{50} assays, using 4 h drug exposure of HT29 and SiHa cells under aerobic and anoxic (H_2/Pd anaerobic chamber) conditions in 96-well plates as described previously.[50] The hypoxic cytotoxicity ratio (HCR) was calculated as the intraexperiment ratio aerobic IC_{50}/anoxic IC_{50} (Tables 1−3).

The relationship between cell killing, drug exposure, and drug metabolism (i.e., the in vitro PK/PD model) was measured as previously described[43,44] by following the clonogenicity of stirred single cell suspensions of HT29 cells for 3 h, at a drug concentration giving approximately one log kill by 1 h, with monitoring of drug concentrations in extracellular medium by HPLC. These concentration−time data were fitted to determine the apparent first-order rate constant for metabolic consumption, k_{met}. The measured parameter values are given in Tables 1−3, and the associated error estimates are tabulated in the Supporting Information. The best fit PK/PD model,[44,48,49] the CT_{10} (area

Scheme 6[a]

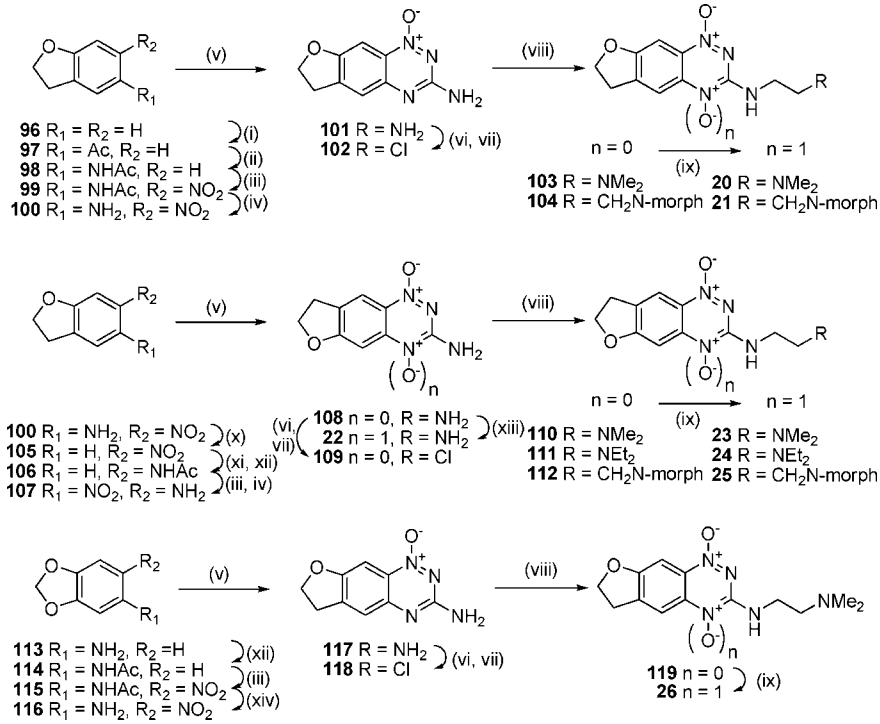

[a] Reagents: (i) $AlCl_3$, AcCl, DCM; (ii) $NH_2OH \cdot HCl$, pyridine, then HCl, Ac_2O, HOAc; (iii) $cHNO_3$, HOAc; (iv) cHCl, EtOH, Δ; (v) NH_2CN, HCl, Δ, then 30% NaOH, Δ; (vi) $NaNO_2$, CF_3CO_2H; (vii) DMF, $POCl_3$, Δ; (viii) $R_2CH_2CH_2NH_2$, DME, Δ; (ix) CF_3CO_3H, CF_3CO_2H, DCM; (x) $NaNO_2$, cH_2SO_4, then H_3PO_2; (xi) H_2, PtO_2, THF, EtOH; (xii) Ac_2O, dioxane; (xiii) CH_3CO_3H, HOAc; (xiv) NaOMe, MeOH, Δ.

Scheme 7[a]

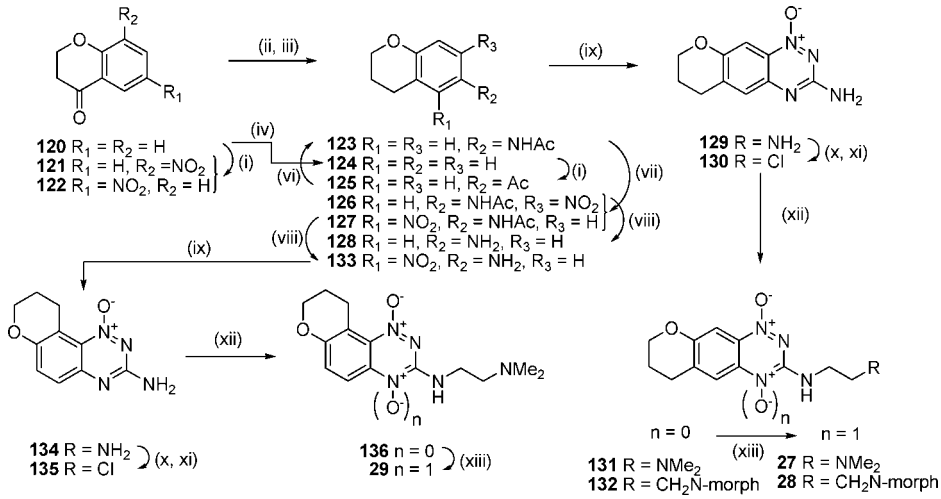

[a] Reagents: (i) KNO_3, cH_2SO_4; (ii) H_2, Pd/C, aq HCl, EtOAc/EtOH; (iii) Ac_2O, dioxane; (iv) Zn, HOAc, Δ; (v) $AlCl_3$, AcCl, DCM; (vi) $NH_2OH \cdot HCl$, pyridine, then HCl, Ac_2O, HOAc; (vii) $fHNO_3$, HOAc; (viii) cHCl, EtOH, Δ; (ix) NH_2CN, HCl, Δ, then 30% NaOH, Δ; (x) $NaNO_2$, CF_3CO_2H; (xi) DMF, $POCl_3$, Δ; (xii) $R_2CH_2CH_2NH_2$, DME, Δ; (xiii) CF_3CO_3H, CF_3CO_2H, DCM.

under the concentration−time curve providing a 10% surviving fraction) and M_{10} (amount of BTO metabolized for a 10% surviving fraction), were estimated by interpolation and are tabulated in the Supporting Information along with the associated error estimates.

Tissue diffusion coefficients, *D*, of six TTOs were measured using HT29 MCLs as previously described under 95% O_2 to suppress bioreductive metabolism.[43] These values, along with previously reported measurements for BTO analogues[44,47] and data for other BTOs (a total of 73 compounds), were used to develop a multiple regression model to calculate *D* for the other analogues as described previously.[48] This model extends the reported[47] dependence, for neutral BTOs, of *D* on logP and molecular weight (MW) by replacing logP with the octanol/water distribution coefficient at pH 7.4 ($logP_{7.4}$) and by adding terms for the numbers of hydrogen bond donors (HD) and acceptors (HA) (eq 1).[67] The calculated and measured values and the associated error estimates are tabulated in the Supporting Information. The calculated values for all TTOs are shown in Tables 1−3.

$$\log(D_{MCL}) = a + b \log MW + \frac{c}{1 + \exp\left(\frac{\log P_{7.4} - x + y \cdot HD + z \cdot HA}{w}\right)} \quad (1)$$

Scheme 8[a]

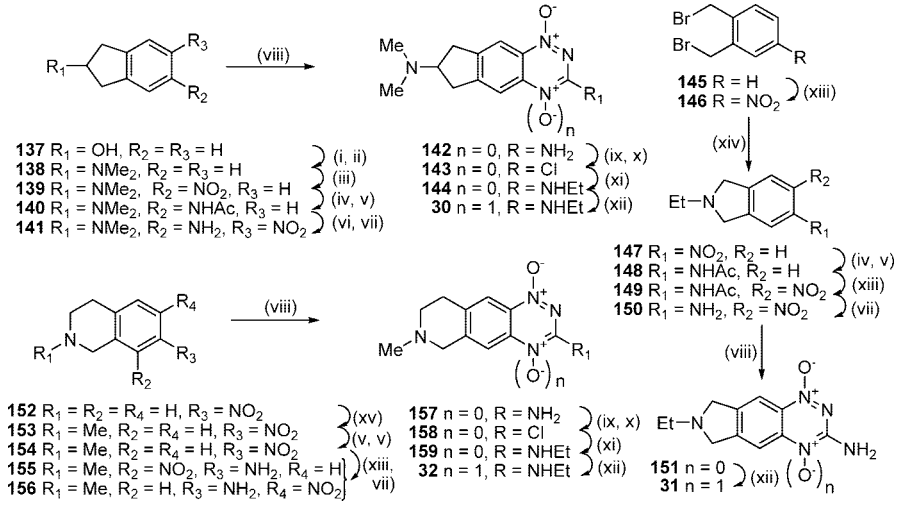

[a] Reagents: (i) MsCl, iPr_2Net, DCM; (ii) aq $NHMe_2$, DMF, Δ; (iii) $cHNO_3$, CF_3CO_2H; (iv) H_2, Pd/C, aq HCl, EtOAc/EtOH; (v) Ac_2O, Et_3N, DCM; (vi) $fHNO_3$, HOAc; (vii) HCl, EtOH, Δ; (viii) NH_2CN, HCl, Δ, then 30% NaOH, Δ; (ix) $NaNO_2$, CF_3CO_2H; (x) DMF, $POCl_3$, Δ; (xi) $EtNH_2$, DME, Δ; (xii) CF_3CO_3H, CF_3CO_2H, DCM; (xiii) KNO_3, cH_2SO_4; (xiv) $EtNH_2 \cdot HCl$, Et_3N, DMF, Δ; (xv) HCO_2H, Ac_2O, THF, then $BH_3 \cdot DMS$.

Scheme 9[a]

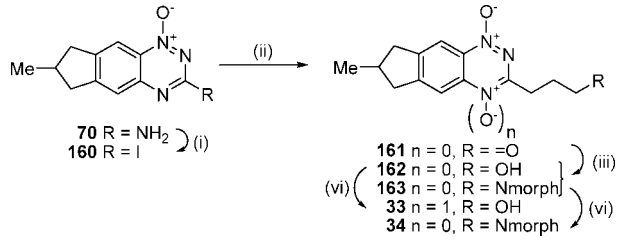

[a] Reagents: (i) *t*-$BuNO_2$, CH_2I_2, CuI, THF, Δ; (ii) AllylOH, $Pd(OAc)_2$, nBu_4NBr, $NaHCO_3$, DMF, Δ; (iii) morpholine, MeOH, then $NaCNBH_3$, HOAc; (iv) CF_3CO_2H, CF_3CO_3H, DCM.

A one-dimensional EVT parameter, the penetration distance into hypoxic tissue assuming planar geometry ($X_{1/2}$, eq 2), was calculated from the opposing effects of D and k_{met} on tissue transport as previously reported,[48] providing a ready comparison between analogues; values are given in Tables 1−3, and the associated error estimates are tabulated in the Supporting Information.

$$X_{1/2} = \ln(2)\sqrt{\frac{D}{k_{met}}} \qquad (2)$$

PK/PD Modeling. The in vivo 3D PK/PD model has been described in detail recently.[45,48] Briefly, transport is modeled in the extravascular compartment of a representative tumor microvascular network by solving the Fick's Second Law diffusion−reaction equations using a Green's function method, providing a description of the PK at each point in the tissue region. The transport parameters used in the model are the tissue diffusion coefficient D (estimated in MCLs) and k_{met} for bioreductive drug metabolism under anoxia (scaled to MCL cell density) determined in vitro as described above. Using the homogeneous PK/PD model established in vitro for each compound, the log cell kill (LCK) was predicted at each position in the tumor microregion. The overall cell kill through the whole region was then calculated for drug only and for drug plus 20 Gy radiation (using the reported radiosensitivity parameters for aerobic and hypoxic HT29 cells).[44] The difference between these [$LCK_{(drug+RAD)} - LCK_{(drug\ alone)}$] gives the model-predicted logs of hypoxic cell kill (LCK_{pred}). The in vitro PK/PD relationship

Scheme 10[a]

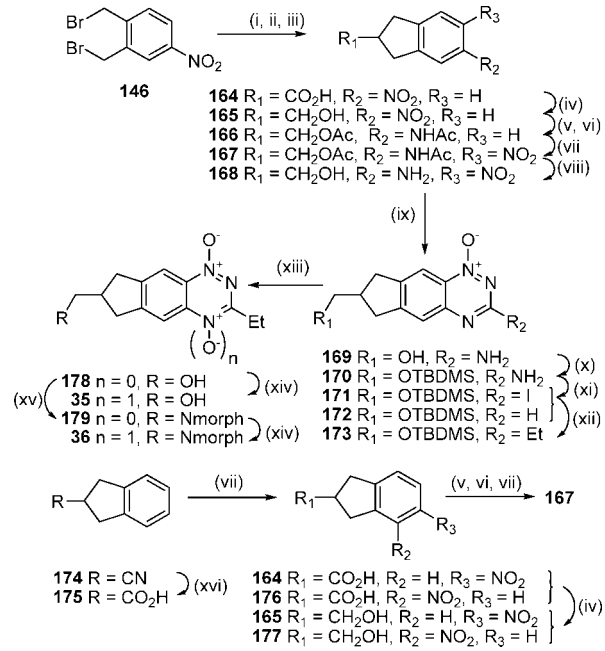

[a] Reagents: (i) NaH, $(EtO_2C)_2CH_2$, Et_2O; (ii) NaOH, EtOH; (iii) xylene, Δ; (iv) $BH_3 \cdot DMS$, THF; (v) H_2, Pd/C, MeOH; (vi) Ac_2O, Et_3N, DCM; (vii) $cHNO_3$, CF_3CO_2H; (viii) 5 M HCl, MeOH, Δ; (ix) NH_2CN, HCl, Δ, then 30% NaOH, Δ; (x) TBDMSCl, iPr_2NEt, DMF; (xi) *t*-$BuNO_2$, CH_2I_2, CuI, THF, Δ; (xii) Et_4Sn, $Pd(PPh_3)_4$, DME, Δ; (xiii) 1 M HCl, MeOH, Δ; (xiv) CF_3CO_3H, DCM; (xv) MsCl, iPr_2NEt, DCM, then morpholine, DMF, Δ; (xvi) cHCl, dioxane, Δ.

was used to predict the area under the plasma concentration−time curve (AUC_{req}) that would be required to give 1 log of cell kill in addition to that produced by a single 20 Gy dose of γ-radiation. In addition, the hypoxic cytotoxicity differential (HCD) is calculated as a measure of hypoxic selectivity in the tumor:

$$HCD = \frac{LCK_{pred} \text{ in the hypoxic region } (<4\mu M\ O_2)}{LCK_{pred} \text{ in the well oxygenated region } (>30\mu M\ O_2)} \qquad (3)$$

where LCK is predicted for the drug alone.

Compounds with high potency (low plasma AUC_{req}) and high in vivo hypoxic selectivity (HCD) have potential to demonstrate improved in vivo hypoxic cell kill compared to TPZ. Comparison using these criteria was made to evaluate the potential of the analogues as improved analogues of TPZ.

Results and Discussion. Targeting the cycloalkane ring systems **3**−**19** (Table 1) using the established benzotriazine ring formation was readily achieved. The cycloalkyl rings conferred increased lipophilicity relative to TPZ. The low solubility of **3** was remedied by addition of an aminoalkylamine at the 3-position, e.g., **4** (Table 1). This effect was general, with only the piperidine **7** failing to show increased solubility.

We have previously demonstrated[48] that replacing the strongly electron-donating 3-NH_2 ($\sigma_p = -0.66$) with the dimethylaminoethylamine side chain raises the one electron reduction potential, $E(1)$, of TPZ by 60 mV. This can be offset by electron-donating substituents at the 6-position, with a 6-Me substituent lowering the $E(1)$ by 40 mV and a 6-OMe substituent, e.g., **2**, lowering the $E(1)$ by 104 mV to a value of −500 mV. Thus, the cycloalkane rings (**4**, **9**, and **19**) lowered the $E(1)$ by ca. 90 mV and the inclusion of a lower pK_a amine (**13**) resulted in a further reduction in $E(1)$.

The fusion of a cycloalkane ring at the 6,7- or 7,8-positions of the BTO nucleus provided TTOs with similar hypoxic cytotoxicity and selectivity to TPZ with the main variation in hypoxic potency resulting from variation in amine side chain pK_a. Thus the morpholides **8**, **13**, and **15** were considerably less potent than more basic analogues. This drop in potency was also reflected in lowered hypoxic metabolism, with the cyclohexyl analogue **17** showing unusually high hypoxic metabolism and potency relative to the other morpholides. The increased lipophilicity from the cycloalkyl rings resulted in increased diffusion relative to TPZ. Consequently, most of these TTOs showed increased EVT as defined by the 1-D transport parameter $X_{1/2}$.

Calculation of the predicted AUC required to achieve 1 log of hypoxic cell kill in tumors (AUC_{req}) and the in vivo hypoxic selectivity (HCD) allowed comparison with previously studied BTO analogues.[48,49] In these studies, analogues with high predicted hypoxic selectivity (HCD) and high predicted in vivo potency (AUC_{req}) were most likely to be active in vivo (upper-left quadrant, Figure 2a). A number of compounds predicted to be active but were not tested because they were structurally similar to other actives (red open upward-pointing triangles). The predicted activity is subject to the in vivo toxicity and plasma pharmacokinetics and in a few examples very low plasma AUC values precluded activity (blue solid downward-pointing triangles). Using these data as a guide (HCD > 6, AUC_{req} < 14000 μM·min), six cycloalkyl-TTOs (**4**, **6**, **8**, **11**, **15**, **17**) demonstrated the potential for in vivo activity (black circles, Figure 2b).

The inclusion of a heteroatom in the fused ring resulted in TTOs with considerably lower lipophilicity than the corresponding cycloalkyl analogues (e.g., compare **20** or **23** with **4**; **27** with **16**) (Table 2). Again the inclusion of a basic side chain conferred excellent aqueous solubility, with the neutral TTO **22** displaying very low solubility. The indanamine **30** was not stable in medium and was not evaluated in vitro.

The oxygen atom of the [3,2-*g*]dihydrofuran **20** had little effect on $E(1)$ compared to **4**, whereas the [2,3-*g*] isomer **23** shows a stronger influence and a similar effect is seen with the dioxole **26** having a similar $E(1)$ to **23** (Table 2). This reflects the stronger electronic influence of substituents at the "6"-position compared to the "7"-position.[50]

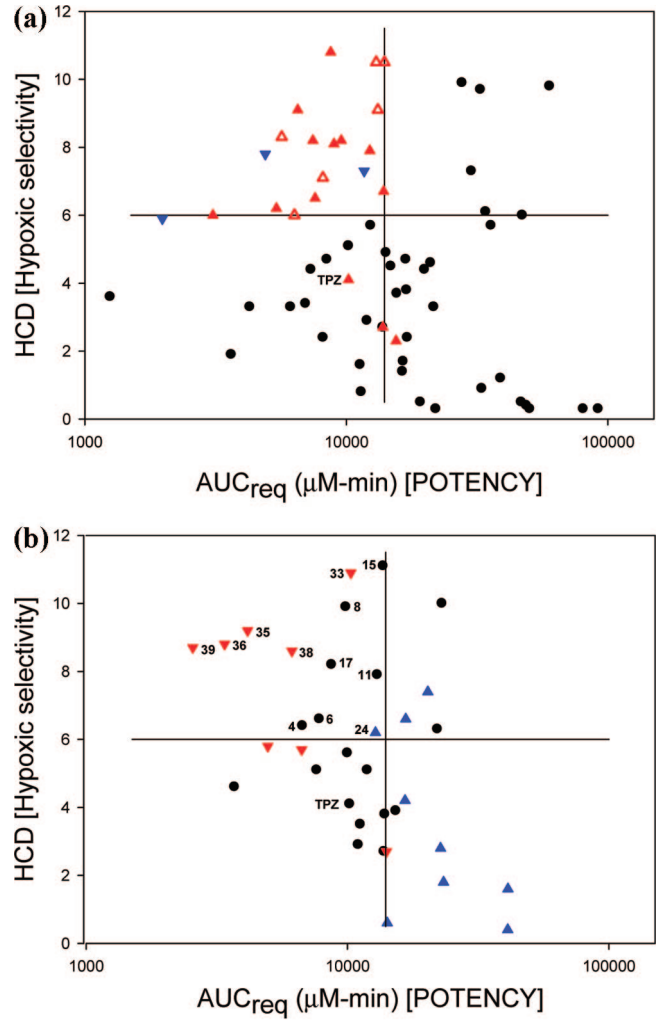

Figure 2. (a) Predicted hypoxic selectivity (HCD) and potency (AUC_{req}) for BTOs. (black circles) Compounds predicted inactive; (red solid upward-pointing triangles) active in vivo; (red open upward-pointing triangles) not tested due to structural similarity to actives; (blue solid downward-pointing triangles) not active in vivo. Data from refs 48 and 49. (b) Predicted hypoxic selectivity (HCD) and potency (AUC_{req}) for TTOs. (black circles) TTOs from Table 1; (blue solid upward-pointing triangles) TTOs from Table 2; (red solid downward-pointing triangles) TTOs from Table 3.

Scheme 11[a]

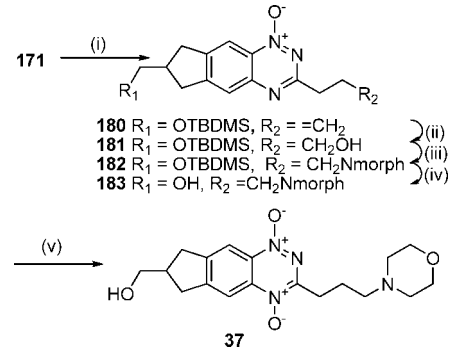

[a] Reagents: (i) $AllylSnBu_3$, $Pd(PPh_3)_4$, DME, Δ; (ii) 9-BBN, THF, then NaOAc, H_2O_2; (iii) MsCl, iPr_2NEt, DCM, then morpholine, DMF; (iv) 1 M HCl, MeOH; (v) CF_3CO_3H, CF_3CO_2H,DCM.

The heterocyclic TTOs showed similar hypoxic potency to TPZ and slightly lower selectivity, with the weakly basic morpholides again displaying reduced potency. The TTO **22** showed low hypoxic potency and selectivity and failed to pass

Scheme 12[a]

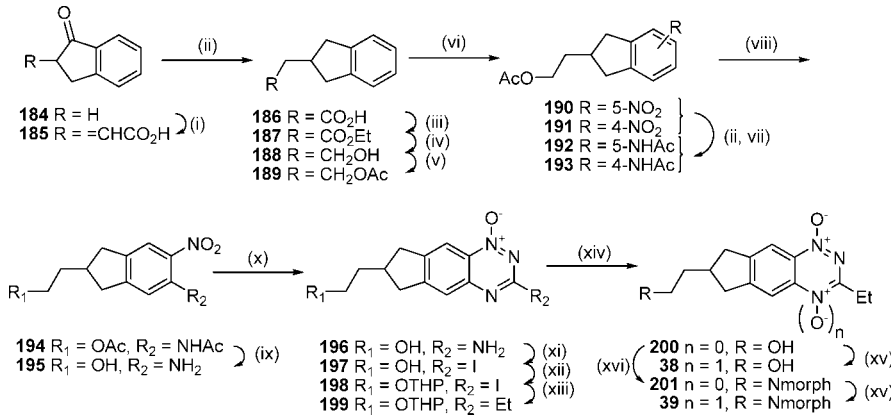

[a] Reagents: (i) 50% aq $HCOCO_2H$, cH_2SO_4, dioxane, Δ; (ii) H_2, Pd/C, MeOH, dioxane; (iii) cH_2SO_4, EtOH; (iv) $LiAlH_4$, THF; (v) Ac_2O, pyridine, DMAP, DCM; (vi) $Cu(NO_3)_2 \cdot 3H_2O$, Ac_2O; (vii) Ac_2O, dioxane; (viii) $cHNO_3$, CF_3CO_2H; (ix) 5 M HCl, MeOH, Δ; (x) NH_2CN, HCl, Δ, then 30% NaOH, Δ; (xi) *t*-$BuNO_2$, I_2, CuI, THF, Δ; (xii) dihydropyran, PPTS, DCM; (xiii) Et_4Sn, $Pd(PPh_3)_4$, DME, Δ; (xiv) $MeSO_3H$, MeOH; (xv) CF_3CO_2H, CF_3CO_3H, DCM; (xvi) MsCl, iPr_2NEt, DCM, then morpholine, DMF, Δ.

the criterion for hypoxic selectivity (HCR > 20) in the PK/PD model[48,49] and was not evaluated further. The decreased lipophilicity of the heterocyclic TTOs **20**−**32** resulted in lowered diffusion, with only the weakly basic amines **28**, **30**, and **32** having *D* values greater than TPZ. The rates of hypoxic metabolism were influenced by the electronic nature of the fused ring and the side chain amine pK_a, with the weakly basic morpholides generally having lower k_{met} values compared to more basic analogues. For TTOs with a 7-oxa atom in the ring, e.g., **20** and **27**, k_{met} values were relatively high, reflecting the weaker dependence of *E*(1) on σ_p for 7-substituents.[50] Only heterocyclic TTOs with very low k_{met} values achieved a balance with the low *D* values, and thus only **21**, **24**, and **25** were predicted to display improved EVT based on their $X_{1/2}$ values. Low hypoxic potency and k_{met} contributed to high AUC_{req} values, which when combined with modest predicted in vivo hypoxic selectivity (HCD) as a consequence of modest *D* values, resulted in only heteroalkyl-TTO **24**, satisfying the criteria for predicted in vivo activity (AUC_{req} < 14000; HCD > 6, blue solid upward-pointing triangle, Figure 2b).

A series of 3-alkyl TTOs **33**−**40** with solubilizing groups attached via the 3-alkyl substituent or the 7-position of the indane ring was prepared. Two examples where the solubilizing moiety was included within the isoquinoline ring (**41**, **42**) were also prepared (Table 3). The strategy was to increase EVT through increased lipophilicity and to optimize the hypoxic metabolism by balancing the electron-donating effects of the fused rings. Replacement of the 3-aminoalkyl substituent with a 3-ethyl group (e.g., **35** compared with **4**) raised the reduction potential by ca. 30 mV, and the inclusion of a morpholine group on the side chain further raised the *E*(1) by ca. 40 mV. A similar elevation of *E*(1) was seen with the morpholide **40** when compared to **21**. Placement of the morpholino group in a remote position off the indane ring (**39**) had a negligible effect on *E*(1).

TTOs **33**−**42** were generally more lipophilic than similar 3-alkylamino analogues, with only the morpholide **40** showing significantly reduced lipophilicity relative to **25** due to the polarity of the dihydrofuran ring. Morpholide side chains provided increased aqueous solubility relative to TPZ, whereas the neutral analogues had reduced solubility. TTO **42** was not evaluated because of instability in culture medium. The neutral TTOs were generally less potent than related analogues bearing morpholide side chains, which had similar hypoxic cytotoxicity to TPZ. TTOs in this series were hypoxia-selective with the exception of **41**, which was not evaluated further. The removal of the 3-NH group resulted in large increases in diffusion coefficient with the addition of a hydrogen bond donor (OH) having a similar negative effect to that of a morpholide group (e.g., compare **33** with **34**, **35** with **36**, and **38** with **39**). Hydrogen bond donors such as hydroxyl groups, although only modestly lowering the $logP_{7.4}$, have a strong negative influence on diffusion rates.[47] The strongly polar nature of the [2,3-*g*]-dihydrofuran moiety dominated in TTO **40**, leading to a low *D* value. The cycloalkyl TTOs **33**−**39** displayed similar rates of hypoxic metabolism to TPZ with the presence of a morpholide side chain, producing a small elevation in k_{met}. The increased diffusion coefficients combined with modest rates of hypoxic metabolism gave significantly increased EVT as defined by $X_{1/2}$. These factors combined to give relatively

Scheme 13[a]

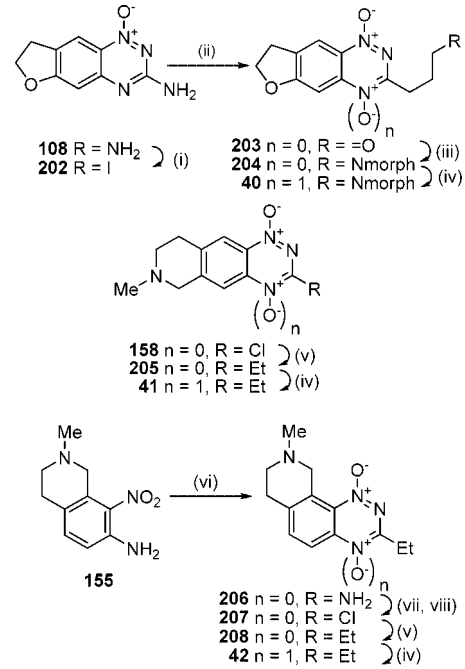

[a] Reagents: (i) *t*-$BuNO_2$, CH_2I_2, CuI, THF, Δ; (ii) allyl alcohol, $Pd(OAc)_2$, nBu_4NBr, $NaHCO_3$, DMF; (iii) morpholine, $NaCNBH_3$, MeOH, DMF; (iv) CF_3CO_3H, CF_3CO_2H, DCM; (v) Et_4Sn, $Pd(PPh_3)_4$, DME, Δ; (vi) NH_2CN, HCl, Δ, then 30% NaOH, Δ; (vii) $NaNO_2$, CF_3CO_2H; (viii) DMF, $POCl_3$, Δ.

Table 1. Physicochemical, in Vitro, and Modelling Parameters for TPZ, BTO **2**, and TTOs **3**−**19**

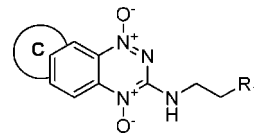

No	Ring C	R_1	pKa[a]	logP$_{7.4}$ calc[b]	Sol.[c] mM	$E(1)$ mV	HT29 IC_{50} hypox μM	HT29 HCR[d]	SiHa IC_{50} hypox μM	SiHa HCR[d]	D calc[e,f]	k_{met}[f,g] min^{-1}	$X_{½}$[f,h] μm	AUC_{req}[i] μM.min	HCD[j]
1[k]	na[l]	na[l]	na[l]	-0.33	9	-456	5.1	71	2.5	107	4.2	0.58	45	10200	4.1
2[k]	na[l]	NMe_2	8.5	-0.07	46	-500	7.7	89	2.9	232	2.9	0.54	35	13800	2.7
3		na[l]	0.0	0.50	3		15.2	27	8.3	31	9.8	0.47	77	22100	6.3
4		NMe_2	8.5	0.42	>51	-486	2.3	152	0.7	111	6.5	0.44	62	6730	6.4
5		NEt_2	9.5	1.29	48		4.1	61	1.1	133	7.4	1.08	45	15300	3.9
6		NPr_2	8.7	0.69	20		2.5	77	0.7	91	19.3	1.07	72	7810	6.6
7		N-piperidine	8.7	1.45	1.9		5.8	49	1.3	143	11.7	1.25	52	3700	4.6
8		CH_2N-morpholine	7.4	1.25	48		21.4	20	8.8	44	9.6	0.19	119	9860	9.9
9		NMe_2	8.5	0.18	>54	-480	3.0	67	1.6	99	8.3	0.74	57	7630	5.1
10		NEt_2	9.5	0.35	>49		4.2	17	0.9	64	9.4	0.97	53	10000	5.6
11		NPr_2	8.7	1.60	40		12.4	7	3.3	23	19.3	0.73	87	13000	7.9
12		N-piperidine	8.7	0.65	36		4.9	53	1.0	51	11.9	1.60	46	13900	3.8
13		CH_2N-morpholine	7.4	0.88	46	-510	38	24	13.9	33	10.3	0.20	122	23000	10.0
14		NMe_2	8.5	0.42	>49		3.5	54	1.4	97	10.2	1.49	44	11000	2.9
15		CH_2N-morpholine	7.4	1.29	>49		19	25	8.4	50	13.8	0.13	173	13700	11.1
16		NMe_2	8.5	0.69							12.8				
17		CH_2N-morpholine	7.4	1.45	49		6.3	25	2.6	54	15.2	0.69	80	8700	8.2
18		NMe_2	8.5	0.69	47		3.4	18	1.0	64	12.8	1.78	46	11200	3.5
19		NMe_2	8.5	1.25	>53	-488	5.2	54	1.2	88	17.7	1.52	58	11900	5.1

[a] Calculated using ACD pK_a. [b] Calculated using ACD logD. [c] Solubility of HCl salts in culture medium. [d] Hypoxia cytotoxicity ratio = oxic IC_{50}/hypoxic IC_{50}. [e] Diffusion coefficient in HT29 MCLs × 10^{-7} cm^2s^{-1}. [f] Error estimates are provided in the Supporting Information. [g] First-order rate constant for metabolism in anoxic HT29 cell suspensions, scaled to the cell density in MCLs. [h] Penetration half-distance in anoxic HT29 tumor tissue (see text). [i] Predicted area under the plasma concentration−time curve required to give 1 log of cell kill in addition to that produced by a single 20 Gy dose of γ radiation. [j] In vivo hypoxic cytotoxicity differential = $LCK_{hypoxic}/LCK_{oxic}$. [k] Data from ref 48. [l] Not applicable.

modest AUC_{req} values and high HCD across the series with TTOs (**33**, **35**, **36**, **38**, **39**) identified as likely to be active in vivo (AUC_{req} < 14000; HCD > 6.0) (red solid downward-pointing triangles, Figure 2b).

The addition of bulky fused rings, either in a linear or angular manner, or the placement of a polar hydroxyl or charged amine solubilizing group in either hemisphere of the molecule resulted in TTOs that were hypoxia-selective. This wide substrate tolerance is consistent with the description of cytochrome P_{450} reductase (CYP450R) as the major reductase responsible for bioactivation of TPZ.[18] CYP450R's prime role is to reduce the cofactor in cytochrome P_{450} and consequently it has a wide cleft allowing access of the substrate enzyme to the active site.[68,69] For this enzyme interaction, electron transfer occurs with minimal overlap of cofactors and is driven by the difference in reduction potential between the substrate and the cofactor.

Table 2. Physicochemical, in Vitro, and Modelling Parameters for TPZ and TTOs **20**−**32**

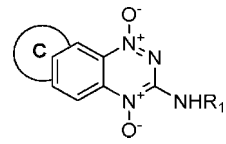

No	Ring C	R_1	pKa[a]	logP$_{7.4}$ calc[b]	Sol.[c] mM	$E(1)$ mV	HT29 IC_{50} hypox μM	HT29 HCR[d]	SiHa IC_{50} hypox μM	SiHa HCR[d]	D calc[e,f]	k_{met}[f,g] min^{-1}	$X_{½}$[f,h] μm	AUC_{req}[i] μM.min	HCD[j]
1[k]	na[l]	H	na[l]	-0.33	9	-456	5.1	71	2.5	107	4.2	0.58	45	10200	4.1
20		$(CH_2)_2NMe_2$	8.5	-1.05	>48	-487	2.4	23	0.30	87	2.6	3.15	20	23300	1.8
21		$(CH_2)_3$N-morpholine	7.4	-0.27	>49		22	8	3.4	28	2.8	0.20	64	20300	7.4
22	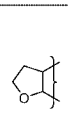	H	na	-0.04	0.1		117	4	23		3.6				
23		$(CH_2)_2NMe_2$	8.5	-1.01	49	-545	5.2	46	1.9	128	2.6	0.60	36	22700	2.8
24		$(CH_2)_2NEt_2$	9.4	-0.68	47		10	113	3.4	122	2.9	0.26	57	12800	6.2
25		$(CH_2)_3$N-morpholine	7.4	-0.27	46		49	6	29	14	2.8	0.23	60	16700	6.6
26		$(CH_2)_2NMe_2$	8.5	-1.09	>50	-541	13	26	5	53	2.3	0.87	28	41100	1.6
27		$(CH_2)_2NMe_2$	8.5	-0.54	>45	-453	1.5	19	0.3	60	3.2	2.43	23	14200	0.6
28		$(CH_2)_3$N-morpholine	7.4	0.48	40		11	19	3.6	41	4.8	0.97	38	29900	33.0
29		$(CH_2)_2NMe_2$	8.5	-0.26	47		4.1	14	0.7	66	3.9	0.59	44	16600	4.2
30		Et	7.6	0.08	46						7.6				
31		H	4.1	-0.57	6	-390	1.5		0.8	80	2.7	2.20	19	41000	0.4
32		Et	5.8	-0.29	>47	-462	2.6	59	1.1	100	5.4				

[a] Calculated using ACD pK_a. [b] Calculated using ACD logD. [c] Solubility of HCl salts in culture medium. [d] Hypoxia cytotoxicity ratio = oxic IC_{50}/hypoxic IC_{50}. [e] Diffusion coefficient in HT29 MCLs × 10^{-7} cm^{2}s^{-1}. [f] Error estimates are provided in the Supporting Information. [g] First-order rate constant for metabolism in anoxic HT29 cell suspensions, scaled to the cell density in MCLs. [h] Penetration half-distance in anoxic HT29 tumor tissue (see text). [i] Predicted area under the plasma concentration−time curve required to give 1 log of cell kill in addition to that produced by a single 20 Gy dose of γ radiation. [j] In vivo hypoxic cytotoxicity differential = $LCK_{hypoxic}/LCK_{oxic}$. [k] Data from ref 48. [l] Not applicable.

Optimization of rates of hypoxic metabolism and tissue diffusion coefficients has been possible for at least 12 different TTO analogues, and these compounds are predicted to be active in vivo. Key to the ongoing development of this class of compounds is the determination of SAR for animal toxicity (maximum tolerated dose) and in vivo pharmacokinetics. The attainment of a sufficiently high C_{max} and AUC has been demonstrated as necessary for activity against hypoxic tumor cells in vivo.[45,48,49] Studies are currently underway with the 12 candidates predicted to be active in vivo to identify SAR for in vivo toxicity and pharmacokinetic parameters.

Conclusions

We have been able to build on previously described SAR to design a wide range of novel tricyclic TTO analogues and explore the effect of these structural modifications on their in vitro activity as hypoxia-selective cytotoxins. A wide range of structural arrangements with cycloalkyl, oxygen-, and nitrogen-containing rings fused in a linear or angular fashion to the benzotriazine core, coupled with neutral, polar, and charged side chains linked to either hemisphere, resulted in TTO analogues that displayed hypoxia-selective cytotoxicity in vitro.

The fused cycloalkyl rings are sufficiently electron-donating in combination with both the 3-aminoalkyl or 3-alkyl substituents to position the one electron reduction potential in an appropriate range for optimal rates of hypoxic metabolism. The stronger electronic and polar influences of the "oxa" rings were more difficult to balance and mostly led to poor EVT properties. The use of amine containing rings or substituents, while providing increased aqueous solubility, provided either unstable TTOs or only modest activity. The lipophilic nature of the cycloalkyl rings also increased lipophilicity and led to increased diffusion coef-

Table 3. Physicochemical, in Vitro, and Modelling Parameters for TPZ and TTOs **33**−**42**

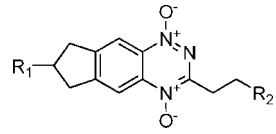

No	R_1	R_2	pKa[a]	logP$_{7.4}$ calc[b]	Sol.[c] mM	E(1) mV	HT29 IC_{50} hypox μM	HT29 HCR[d]	SiHa IC_{50} hypox μM	SiHa HCR[d]	D calc[e,f]	k_{met}[f,g] min^{-1}	$X_{½}$[f,h] μm	AUC_{req}[i] μM.min	HCD[j]
1[k]	na[l]	na[l]	na[l]	-0.33	9	-456	5.1	71	2.5	107	4.2	0.58	45	10200	4.1
33	CH_3	CH_2OH	0.0	1.14	10		13.0	80	8.0	104	21.0	0.24	158	10300	10.9
34	CH_3	CH_2N-morpholine	7.1	0.99	36		2.9	72	1.7	134	21.0	0.96	80	4960	5.8
35	CH_2OH	H	0.0	0.69	5	-452	17	45	6.5	48	17.7	0.47	104	4150	9.2
36	CH_2N-morpholine	H	7.0	0.29	43		4.8	31	2.4	62	17.3	0.54	96	3390	8.8
37	CH_2OH	CH_2N-morpholine	7.1	-0.18	48	-408	2.4	121	1.8	206	3.8	0.90	35	14100	2.7
38	$(CH_2)_2OH$	H	na	0.50	2		7.7	102	2.9	86	15.4	0.54	91	6130	8.6
39	$(CH_2)_3$N-morpholine	H	7.5	0.50	>51	-431	3.6	36	1.3	84	18.5	0.54	100	2560	8.7
40		CH_2N-morpholine	7.1	-1.30	51	-468	8.9	25	5.1	43	3.5	0.31	57	6680	5.7
41		H	5.8	0.09	>47	-344	13.1	2	3.1	6	20.9				
42		H	5.2	0.19											

[a] Calculated using ACD pK_a. [b] Calculated using ACD logD. [c] Solubility of HCl salts in culture medium. [d] Hypoxia cytotoxicity ratio = oxic IC_{50}/hypoxic IC_{50}. [e] Diffusion coefficient in HT29 MCLs × 10^{-7} cm^2s^{-1}. [f] Error estimates are provided in the Supporting Information. [g] First-order rate constant for metabolism in anoxic HT29 cell suspensions, scaled to the cell density in MCLs. [h] Penetration half-distance in anoxic HT29 tumor tissue (see text). [i] Predicted area under the plasma concentration−time curve required to give 1 log of cell kill in addition to that produced by a single 20 Gy dose of γ radiation. [j] In vivo hypoxic cytotoxicity differential = $LCK_{hypoxic}/LCK_{oxic}$. [k] Data from ref 48. [l] Not applicable.

ficients, which when combined with weakly basic morpholine side chains gave the best balance of solubility and increased diffusion.

The selection was further refined using PK/PD model predictions of the AUC_{req} and HCD and 12 TTOs were predicted to be active in vivo subject to adequate plasma pharmacokinetics.

Experimental Section

Chemistry. General experimental details are described in the Supporting Information. TPZ and BTO **2** were synthesized as previously described.[48]

Example of Synthetic Methods. See Supporting Information for full experimental details.

Preparation of 3-Aminotriazine 1-Oxides: Method (i), Scheme 1. A mixture of nitroaniline (20 mmol) and cyanamide (80 mmol) were mixed together at 100 °C, cooled to 50 °C, cHCl (10 mL) added dropwise (CAUTION: exotherm), and the mixture heated at 100 °C for 4 h. The mixture was cooled to 50 °C, 7.5 M NaOH solution added until the mixture was strongly basic, and the mixture stirred at 100 °C for 3 h. The mixture was cooled, diluted with water (100 mL), filtered, washed with water (3 × 30 mL), washed with ether (2 × 5 mL), and dried. If necessary, the residue was purified by chromatography, eluting with a gradient (0−10%) of MeOH/DCM, to give the 1-oxide.

Preparation of 3-Chlorotriazine 1-Oxides: Methods (iii, iv), Scheme 1. Sodium nitrite (10 mmol) was added in small portions to a stirred solution of 1-oxide (5 mmol) in trifluoroacetic acid (20 mL) at 0 °C, and the solution was stirred at 20 °C for 3 h. The solution was poured into ice/water, stirred for 30 min, filtered, washed with water (3 × 10 mL), and dried. The solid was suspended in $POCl_3$ (20 mL) and DMF (0.2 mL) and stirred at 100 °C for 1 h. The solution was cooled, poured into ice/water, stirred for 30 min, filtered, washed with water (3 × 30 mL), and dried. The solid was suspended in DCM (150 mL), dried, and the solvent evaporated. The residue was purified by chromatography, eluting with 5% EtOAc/DCM, to give the chloride.

Preparation of 3-alkylamino 1-Oxides: Method (vi), Scheme 1. Amine (3.0 mmol) was added to a stirred solution of chloride (1.0 mmol) in DME (50 mL) and the solution stirred at reflux temperature for 8 h. The solution was cooled to 20 °C, the solvent evaporated, and the residue partitioned between aqueous NH_4OH solution (100 mL) and EtOAc (100 mL). The organic fraction was dried and the solvent evaporated. The residue was purified by chromatography, eluting with a gradient (0−10%) of MeOH/DCM, to give the 1-oxide.

Preparation of 1-Oxides: Method (vii), Scheme 1. $Pd(PPh_3)_4$ (0.1 mmol) was added to a stirred, degassed solution of halide (2.0 mmol) and stannane (2.4 mmol) in DME (20 mL), and the solution was stirred under N_2 at reflux temperature for 16 h. The solvent was evaporated, and the residue was dissolved in DCM (10 mL) and stirred with saturated aqueous KF solution (10 mL) for 30 min. The mixture was filtered through celite, the celite was washed with DCM, and the combined organic filtrate was washed with water. The organic fraction was dried, the solvent evaporated, and the residue purified by chromatography, eluting with DCM to give product, which was, if necessary, further purified by chromatography, eluting with 20% EtOAc/petroleum ether, to give the 3-alkyl 1-oxide.

Preparation of 1,4-Dioxides 3−42: Method (vii), Scheme 1. Hydrogen peroxide (70%, 10 mmol) was added dropwise to a stirred solution of trifluoroacetic anhydride (10 mmol) in DCM (20 mL) at 0 °C. The mixture was stirred at 0 °C for 5 min, warmed to 20 °C, stirred for 10 min, and cooled to 5 °C. The mixture was added to a stirred solution of 1-oxide (1.0 mmol) [and where aliphatic amine side chains are present, TFA (5.0 mmol)] in DCM (15 mL) at 0 °C, and the mixture was stirred at 20 °C for 4−16 h. The solution was carefully diluted with water (20 mL) and the mixture made basic with aqueous NH_4OH solution, and the mixture was stirred for 15 min and then extracted with $CHCl_3$ (5 × 50 mL). The organic fraction was dried and the solvent evaporated. The residue was purified by chromatography, eluting with a gradient (0−15%) of MeOH/DCM, to give 1,4-dioxides.

Acknowledgment. We thank Jane Botting, Dr. Maruta Boyd, Alison Hogg, Sisira Kumara, and Sarath Liyanage, for technical assistance. We thank Degussa Peroxide Ltd, Morrinsville, New Zealand for the generous gift of 70% hydrogen peroxide. This work was supported by the U.S. National Cancer Institute under grant CA82566 (M.P.H., K.P., K.O.H., F.B.P., W.R.W., W.AD.), the Health Research Council of New Zealand (W.R.W., R.F.A., S.S.S.), and the Auckland Division of the Cancer Society of New Zealand (W.A.D.). Further support from Proacta Therapeutics Ltd (H.H.L.) and the Australian Institute of Nuclear Sciences and Engineering is acknowledged.

Supporting Information Available: Experimental details and characterization data for synthetic intermediates **43**−**208** and TTOs **3**−**42**; experimental details for the physicochemical and biological methods; tables of physicochemical and in vitro data with estimates of errors. This material is available free of charge via the Internet at http://pubs.acs.org.

References

(1) Semenza, G. L. HIF-1 mediates the Warburg effect in clear cell renal carcinoma. *J. Bioenerg. Biomembr.* **2007**, *39*, 231–234.
(2) Gatenby, R. A.; Gillies, R. J. Glycolysis in cancer: a potential target for therapy. *Int. J. Biochem. Cell Biol.* **2007**, *39*, 1358–1366.
(3) Harris, A. L. Hypoxia—a key regulatory factor in tumour growth. *Nature Rev. Cancer* **2002**, *2*, 38–47.
(4) Semenza, G. L. HIF-1 and tumor progression: pathophysiology and therapeutics. *Trends Mol. Med.* **2002**, *8*, S62–S67.
(5) Pennachietti, S.; Michieli, P.; Galluzzo, M.; Mazzone, M.; Giordano, S.; Comoglio, P. M. Hypoxia promotes invasive growth by transcriptional activation of the met protooncogene. *Cancer Cell* **2003**, *3*, 347–361.
(6) Cairns, R. A.; Hill, R. P. Acute hypoxia enhances spontaneous lymph node metastasis in an orthotopic murine model of human cervical carcinoma. *Cancer Res.* **2004**, *64*, 2054–2061.
(7) Subarsky, P.; Hill, R. P. The hypoxic tumour microenvironment and metastatic progression. *Clin. Exp. Metastases* **2003**, *20*, 237–250.
(8) Durand, R. E. The influence of microenvironmental factors during cancer therapy. *In Vivo* **1994**, *8*, 691–702.
(9) Tannock, I. F. Conventional cancer therapy: promise broken or promise delayed? *Lancet* **1998**, *351*, 9–16.
(10) Brown, J. M.; Wilson, W. R. Exploiting tumor hypoxia in cancer treatment. *Nature Rev. Cancer* **2004**, *4*, 437–447.
(11) Nordsmark, M.; Overgaard, M.; Overgaard, J. Pretreatment oxygenation predicts radiation response in advanced squamous cell carcinoma of the head and neck. *Radiother. Oncol.* **1996**, *41*, 31–39.
(12) Fyles, A. W.; Milosevic, M.; Wong, R.; Kavanagh, M. C.; Pintilie, M.; Sun, A.; Chapman, W.; Levin, W.; Manchul, L.; Keane, T. J.; Hill, R. P. Oxygenation predicts radiation response and survival in patients with cervix cancer. *Radiother. Oncol.* **1998**, *48*, 149–156.
(13) Koukourakis, M. I.; Bentzen, S. M.; Giatromanolaki, A.; Wilson, G. D.; Daley, F. M.; Saunders, M. I.; Dische, S.; Sivridis, E.; Harris, A. L. Endogenous markers of two separate hypoxia response pathways (hypoxia inducible factor 2 alpha and carbonic anhydrase 9) are associated with radiotherapy failure in head and neck cancer patients recruited in the CHART randomized trial. *J. Clin. Oncol.* **2006**, *24*, 727–735.
(14) Denny, W. A.; Wilson, W. R.; Hay, M. P. Recent developments in the design of bioreductive drugs. *Br. J. Cancer* **1996**, *74*, S32–S38.
(15) Brown, J. M.; Giaccia, A. J. The unique physiology of solid tumors: opportunities (and problems) for cancer therapy. *Cancer Res.* **1998**, *58*, 1408–1416.
(16) Brown, J. M. SR 4233 (tirapazamine): a new anticancer drug exploiting hypoxia in solid tumours. *Br. J. Cancer* **1993**, *67*, 1163–1170.
(17) Denny, W. A.; Wilson, W. R. Tirapazamine: a bioreductive anticancer drug that exploits tumour hypoxia. *Expert Opin. Invest. Drugs* **2000**, *9*, 2889–2901.
(18) Patterson, A. V.; Saunders, M. P.; Chinje, E. C.; Patterson, L. H.; Stratford, I. J. Enzymology of tirapazamine metabolism: a review. *Anti-Cancer Drug Des.* **1998**, *13*, 541–573.
(19) Anderson, R. F.; Shinde, S. S.; Hay, M. P.; Gamage, S. A.; Denny, W. A. Activation of 3-amino-1,2,4-benzotriazine 1,4-dioxide antitumor agents to oxidizing species following their one-electron reduction. *J. Am. Chem. Soc.* **2003**, *125*, 748–756.
(20) Shinde, S. S.; Anderson, R. F.; Hay, M. P.; Gamage, S. A.; Denny, W. A. Oxidation of 2-deoxyribose by benzotriazinyl radicals of antitumor 3-amino-1,2,4-benzotriazine 1,4-dioxides. *J. Am. Chem. Soc.* **2004**, *126*, 7853–7864.
(21) Daniels, J. S.; Gates, K. S. DNA cleavage by the antitumor agent 3-amino-1,2,4-benzotriazine 1,4-dioxide (SR4233). Evidence for involvement of hydroxyl radical. *J. Am. Chem. Soc.* **1996**, *118*, 3380–3385.
(22) Chowdhury, G.; Junnotula, V.; Daniels, J. S.; Greenberg, M. M.; Gates, K. S. DNA strand damage product analysis provides evidence that the tumor cell-specific cytotoxin tirapazamine produces hydroxyl radical and acts as a surrogate for O_2. *J. Am. Chem. Soc.* **2007**, *129*, 12870–12877.
(23) Wang, J.; Biedermann, K. A.; Brown, J. M. Repair of DNA and chromosome breaks in cells exposed to SR 4233 under hypoxia or to ionizing radiation. *Cancer Res.* **1992**, *52*, 4473–4477.
(24) Siim, B. G.; van Zijl, P. L.; Brown, J. M. Tirapazamine-induced DNA damage measured using the comet assay correlates with cytotoxicity towards hypoxic tumour cells in vitro. *Br. J. Cancer* **1996**, *73*, 952–960.
(25) Siim, B. G.; Menke, D. R.; Dorie, M. J.; Brown, J. M. Tirapazamine-induced cytotoxicity and DNA damage in transplanted tumors: relationship to tumor hypoxia. *Cancer Res.* **1997**, *57*, 2922–2928.
(26) Peters, K. B.; Brown, J. M. Tirapazamine: A Hypoxia-Activated Topoisomerase II Poison. *Cancer Res.* **2002**, *62*, 5248–5253.
(27) Evans, J. W.; Chernikova, S. B.; Kachnic, L. A.; Banath, J. P.; Sordet, O.; Delahoussaye, Y. M.; Treszezamsky, A.; Chon, B. H.; Feng, Z.; Gu, Y.; Wilson, W. R.; Pommier, Y.; Olive, P. L.; Powell, S. N.; Brown, J. M. Homologous recombination is the principal pathway for the repair of DNA damage induced by tirapazamine in mammalian cells. *Cancer Res.* **2008**, *68*, 257–265.
(28) Brown, J. M.; Lemmon, M. J. Potentiation by the hypoxic cytotoxin SR 4233 of cell killing produced by fractionated irradiation of mouse tumors. *Cancer Res.* **1990**, *50*, 7745–7459.
(29) Brown, J. M.; Lemmon, M. J. Tumor hypoxia can be exploited to preferentially sensitize tumors to fractionated irradiation. *Int. J. Radiat. Oncol., Biol., Phys.* **1991**, *20*, 457–461.
(30) Dorie, M. J.; Brown, J. M. Tumor-specific, schedule-dependent interaction between tirapazamine (SR 4233) and cisplatin. *Cancer Res.* **1993**, *53*, 4633–4636.
(31) Dorie, M. J.; Brown, J. M. Modification of the antitumor activity of chemotherapeutic drugs by the hypoxic cytotoxic agent tirapazamine. *Cancer Chemother. Pharmacol.* **1997**, *39*, 361–366.
(32) Marcu, L.; Olver, I. Tirapazamine: From Bench to Clinical Trials. *Curr. Clin. Pharmacol.* **2006**, *1*, 71–79.
(33) Rischin, D.; Fisher, R.; Peters, L.; Corry, J.; Hicks, R. Hypoxia in head and neck cancer: studies with hypoxic positron emission tomography and hypoxic cytotoxins. *Int. J. Radiat. Oncol., Biol., Phys.* **2007**, *69*, S61–S63.

(34) Rischin, D.; Peters, L.; O'Sullivan, B.; Giralt, J.; Yuen, K.; Trotti, A.; Bernier, J.; Bourhis, J.; Henke, M.; Fisher, R. Phase III study of tirapazamine, cisplatin and radiation versus cisplatin and radiation for advanced squamous cell carcinoma of the head and neck. *J. Clin. Oncol.* **2008**, *26*, abstract LBA6008.

(35) Rischin, D.; Hicks, R. J.; Fisher, R.; Binns, D.; Corry, J.; Porceddu, S.; Peters, L. J. Prognostic significance of [18F]-misonidazole positron emission tomography-detected tumor hypoxia in patients with advanced head and neck cancer randomly assigned to chemoradiation with or without tirapazamine: a substudy of Trans-Tasman Radiation Oncology Group Study 98.02. *J. Clin. Oncol.* **2006**, *24*, 2098–2104.

(36) Peters, L.; Rischin, D.; Fisher, R.; Corry, J.; Hicks, R. Identification and therapeutic targeting of hypoxia in H&N cancer. *Int. Congr. Radiat. Res.* **2007**,

(37) Rischin, D.; Peters, L.; Fisher, R.; Macann, A.; Denham, J.; Poulsen, M.; Jackson, M.; Kenny, L.; Penniment, M.; Corry, J.; Lamb, D.; McClure, B. Tirapazamine, cisplatin, and radiation versus fluorouracil, cisplatin, and radiation in patients with locally advanced head and neck cancer: a randomized phase II trial of the Trans-Tasman Radiation Oncology Group (TROG 98.02). *J. Clin. Oncol.* **2005**, *23*, 79–87.

(38) Durand, R. E.; Olive, P. L. Physiologic and cytotoxic effects of tirapazamine in tumor-bearing mice. *Radiat. Oncol. Invest.* **1997**, *5*, 213–219.

(39) Durand, R. E.; Olive, P. L. Evaluation of bioreductive drugs in multicell spheroids. *Int. J. Radiat. Oncol, Biol., Phys.* **1992**, *22*, 689–692.

(40) Hicks, K. O.; Fleming, Y.; Siim, B. G.; Koch, C. J.; Wilson, W. R. Extravascular diffusion of tirapazamine: effect of metabolic consumption assessed using the multicellular layer model. *Int. J. Radiat. Oncol., Biol., Phys.* **1998**, *42*, 641–649.

(41) Kyle, A. H.; Minchinton, A. I. Measurement of delivery and metabolism of tirapazamine to tumour tissue using the multilayered cell culture model. *Cancer Chemother. Pharmacol.* **1999**, *43*, 213–220.

(42) Baguley, B. C.; Hicks, K. O.; Wilson, W. R. Tumour cell cultures in drug development. In *Anticancer Drug Development*; Baguley, B. C.; Kerr, D. J., Eds.; Academic Press: San Diego, 2002; pp 269−284.

(43) Hicks, K. O.; Pruijn, F. B.; Sturman, J. R.; Denny, W. A.; Wilson, W. R. Multicellular resistance to tirapazamine is due to restricted extravascular transport: a pharmacokinetic/pharmacodynamic study in multicellular layers. *Cancer Res.* **2003**, *63*, 5970–5977.

(44) Hicks, K. O.; Siim, B. G.; Pruijn, F. B.; Wilson, W. R. Oxygen dependence of the metabolic activation and cytotoxicity of tirapazamine: implications for extravascular transport and activity in tumors. *Radiat. Res.* **2004**, *161*, 656–666.

(45) Hicks, K. O.; Pruijn, F. B.; Secomb, T. W.; Hay, M. P.; Hsu, R.; Brown, J. M.; Denny, W. A.; Dewhirst, M. W.; Wilson, W. R. Use of three-dimensional tissue cultures to model extravascular transport and predict in vivo activity of hypoxia-targeted anticancer drugs. *J. Natl. Cancer Inst.* **2006**, *98*, 1118–1128.

(46) Hicks, K. O.; Myint, H.; Patterson, A. V.; Pruijn, F. B.; Siim, B. G.; Patel, K.; Wilson, W. R. Oxygen dependence and extravascular transport of hypoxia-activated prodrugs: comparison of the dinitrobenzamide mustard PR-104A and tirapazamine. *Int. J. Radiat. Oncol., Biol., Phys.* **2007**, *69*, 560–571.

(47) Pruijn, F. B.; Sturman, J.; Liyanage, S.; Hicks, K. O.; Hay, M. P.; Wilson, W. R. Extravascular transport of drugs in tumor tissue: effect of lipophilicity on diffusion of tirapazamine analogues in multicellular layer cultures. *J. Med. Chem.* **2005**, *48*, 1079–1087.

(48) Hay, M. P.; Hicks, K. O.; Pruijn, F. B.; Pchalek, K.; Siim, B. G.; Wilson, W. R.; Denny, W. A. Pharmacokinetic/pharmacodynamic model-guided identification of hypoxia-selective 1,2,4-benzotriazine 1,4-dioxides with antitumor activity: the role of extravascular transport. *J. Med. Chem.* **2007**, *50*, 6392–6404.

(49) Hay, M. P.; Pchalek, K.; Pruijn, F. B.; Hicks, K. O.; Siim, B. G.; Anderson, R. R.; Shinde, S. S.; Phillips, V.; Denny, W. A.; Wilson, W. R. Hypoxia-selective 3-alkyl 1,2,4-benzotriazine 1,4-dioxides: the influence of hydrogen bond donors on extravascular transport and antitumor activity. *J. Med. Chem.* **2007**, *50*, 6654–6664.

(50) Hay, M. P.; Gamage, S. A.; Kovacs, M. S.; Pruijn, F. B.; Anderson, R. F.; Patterson, A. V.; Wilson, W. R.; Brown, J. M.; Denny, W. A. Structure−activity relationships of 1,2,4-benzotriazine 1,4-dioxides as hypoxia-selective analogues of tirapazamine. *J. Med. Chem.* **2003**, *46*, 169–182.

(51) Zeman, E. M.; Baker, M. A.; Lemmon, M. J.; Pearson, C. I.; Adams, J. A.; Brown, J. M.; Lee, W. W.; Tracy, M. Structure−activity relationships for benzotriazine di-*N*-oxides. *Int. J. Radiat. Oncol., Biol., Phys.* **1989**, *16*, 977–981.

(52) Minchinton, A. I.; Lemmon, M. J.; Tracy, M.; Pollart, D. J.; Martinez, A. P.; Tosto, L. M.; Brown, J. M. Second-generation 1,2,4-benzotriazine 1,4-di-*N*-oxide bioreductive antitumor agents: pharmacology and activity in vitro and in vivo. *Int. J. Radiat. Oncol., Biol., Phys* **1992**, *22*, 701–705.

(53) Kelson, A. B.; McNamara, J. P.; Pandey, A.; Ryan, K. J.; Dorie, M. J.; McAfee, P. A.; Menke, D. R.; Brown, J. M.; Tracy, M. 1,2,4-Benzotriazine 1,4-dioxides. An important class of hypoxic cytotoxins with antitumor activity. *Anti-Cancer Drug Des.* **1998**, *13*, 575–592.

(54) Jiang, F.; Yang, B.; Fan, L.; Heb, Q.; Hu, Y. Synthesis and hypoxic-cytotoxic activity of some 3-amino-1,2,4-benzotriazine-1,4-dioxide derivatives. *Bioorg. Med. Chem. Lett.* **2006**, *16*, 4209–4213.

(55) Jiang, F.; Weng, Q.; Sheng, R.; Xia, Q.; He, Q.; Yang, B.; Hu, Y. Synthesis, structure and hypoxic cytotoxicity of 3-amino-1,2,4-benzotriazine-1,4-dioxide derivatives. *Arch. Pharm. (Weinheim, Ger.)* **2007**, *340*, 258–263.

(56) Cerecetto, H.; Gonzalez, M.; Onetto, S.; Saenz, P.; Ezpeleta, O.; De Cerain, A. L.; Monge, A. 1,2,4-Triazine *N*-oxide derivatives: studies as potential hypoxic cytotoxins. Part II. *Arch. Pharm. (Weinheim, Ger.)* **2004**, *337*, 247–258.

(57) Cerecetto, H.; Gonzalez, M.; Risso, M.; Saenz, P.; Olea-Azar, C.; Bruno, A. M.; Azqueta, A.; De Cerain, A. L.; Monge, A. 1,2,4-Triazine *N*-oxide derivatives: Studies as potential hypoxic cytotoxins. Part III. *Arch. Pharm. (Weinheim, Ger.)* **2004**, *337*, 271–280.

(58) Monge, A.; Palop, J. A.; Gonzalez, M.; Martinez-Crespo, F. J.; De Cerain, A. L.; Sainz, Y.; Narro, S.; Barker, A. J.; Hamilton, E. New hypoxia-selective cytotoxins derived from quinoxaline 1,4-dioxides. *J. Hetercycl. Chem.* **1995**, *32*, 1213–1217.

(59) Monge, A.; Palop, J. A.; De Cerain, A. L.; Senador, V.; Martinez-Crespo, F. J.; Sainz, Y.; Narro, S.; Garcia, E.; de Miguel, C.; Gonzalez, M. Hypoxia-selective agents derived from quinoxaline 1,4-di-*N*-oxides. *J. Med. Chem.* **1995**, *38*, 1786–1792.

(60) Monge, A.; Martinez-Crespo, F. J.; De Cerain, A. L.; Palop, J. A.; Narro, S.; Senador, V.; Marin, A.; Sainz, Y.; Gonzalez, M.; Hamilton, E. Hypoxia-selective agents derived from 2-quinoxalinecarbonitrile 1,4-di-*N*-oxides. 2. *J. Med. Chem.* **1995**, *38*, 4488–4494.

(61) Amin, K. M.; Ismail, M. M. F.; Noaman, E.; Soliman, D. H.; Ammard, Y. A. New quinoxaline 1,4-di-*N*-oxides, Part 1: Hypoxia-selective cytotoxins and anticancer agents derived from quinoxaline1,4-di-*N*-oxides. *Bioorg. Med. Chem.* **2006**, *14*, 6917−6923.

(62) Hay, M. P.; Denny, W. A. A new and versatile synthesis of 3-alkyl-1,2,4-benzotriazine-1,4-dioxides: preparation of the bioreductive cytotoxins SR4895 and SR4941. *Tetrahedron Lett.* **2002**, *43*, 9569–9571.

(63) Pchalek, K.; Hay, M. P. Stille Coupling Reactions in the Synthesis of Hypoxia-Selective 3-Alkyl-1,2,4-Benzotriazine 1,4-Dioxide Anticancer Agents. *J. Org. Chem.* **2006**, *71*, 6530–6535.

(64) Anderson, R. F.; Denny, W. A.; Li, W.; Packer, J. E.; Tercel, M.; Wilson, W. R. Pulse radiolysis studies on the fragmentation of arylmethyl quaternary nitrogen mustards upon their one-electron reduction in aqueous solution. *J. Phys. Chem. A* **1997**, *101*, 9704–9709.

(65) Wardman, P. Reduction potentials of one-electron couples involving free radicals in aqueous solution. *J. Phys. Chem. Ref. Data* **1989**, *18*, 1637–1755.

(66) Siim, B. G.; Hicks, K. O.; Pullen, S. M.; van Zijl, P. L.; Denny, W. A.; Wilson, W. R. Comparison of aromatic and tertiary amine *N*-oxides of acridine DNA intercalators as bioreductive drugs−cytotoxicity, DNA binding, cellular uptake, and metabolism. *Biochem. Pharmacol.* **2000**, *60*, 969–978.

(67) Pruijn, F. B.; Patel, K.; Hay, M. P.; Wilson, W. R.; Hicks, K. O. Prediction of Tumour Tissue Diffusion Coefficients of Hypoxia-Activated Prodrugs from Physicochemical Parameters. *Aust. J. Chem.* **2008**, *61*, 687–693.

(68) Wang, M.; Roberts, D. L.; Paschke, R.; Shea, T. M.; Masters, B. S. S.; Kim, J-J. P. Three-dimensional structure of NADPH-cytochrome P450reductase: prototype for FMN- and FAD-containing enzymes. *Proc. Natl. Acad. Sci. U.S.A.* **1997**, *94*, 8411–8416.

(69) Zhao, Q.; Modi, S.; Smith, G.; Paine, M.; Mcdonagh, P. D.; Wolf, C. R.; Tew, D.; Lian, L.-Y.; Roberts, G. C. K.; Driessen, H. P. C. Crystal structure of the FMN-binding domain of human cytochrome P450 reductase at 1.93 Å resolution. *Protein Sci.* **1999**, *8*, 298–306.

JM800967H